Materials Today Bio 16 (2022) 100440

Contents lists available at ScienceDirect

Materials Today Bio

journal homepage: www.journals.elsevier.com/materials-today-bio

DNA aerogels and DNA-wrapped CNT aerogels for neuromorphic applications

Mahshid Hosseini [a,b], Vahid Rahmanian [c], Tahira Pirzada [c], Nikolay Frick [a], Abhichart Krissanaprasit [a], Saad A. Khan [c,*], Thomas H. LaBean [a,**]

[a] Department of Materials Science and Engineering, North Carolina State University, Raleigh, NC, USA
[b] Department of Physics, North Carolina State University, Raleigh, NC, USA
[c] Department of Chemical and Biomolecular Engineering, North Carolina State University, Raleigh, NC, USA

ARTICLE INFO

Keywords:
DNA aerogel
DNA-wrapped CNT aerogel
Resistive switching
Neuromorphic application
Self-assembly

ABSTRACT

Nucleic acids are programmable materials that can self-assemble into defined or stochastic three-dimensional network architectures. Various attributes of self-assembled, cross-linked Deoxyribonucleic acid (DNA) hydrogels have recently been investigated, including their mechanical properties and potential biomedical functions. Herein, for the first time, we describe the successful construction of pure DNA aerogels and DNA-wrapped carbon nanotube (CNT) composite (DNA-CNT) aerogels via a single-step freeze-drying of the respective hydrogels. These aerogels reveal highly porous and randomly branched structures with low density. The electrical properties of pure DNA aerogel mimic that of a simple capacitor; in contrast, the DNA-CNT aerogel displays a fascinating resistive switching behavior in response to an applied bias voltage sweep reminiscent of a volatile memristor. We believe these novel aerogels can serve as a platform for developing complex biomimetic devices for a wide range of applications, including real-time computation, neuromorphic computing, biochemical sensing, and biodegradable functional implants. More importantly, insight obtained here on self-assembling DNA to create aerogels will pave the way to construct novel aerogel-based material platforms from DNA coated or wrapped functional entities.

With its ability to undergo molecular self-assembly, DNA is a promising, programmable nanomaterial that has been used to construct sophisticated two- and three-dimensional materials [1–4]. Structural folding information encoded in DNA has been used to form not only specific, well-defined nanostructures but also network microstructures with a significant random character, for example, DNA hydrogels [5]. In 2006, Luo and colleagues reported a method for construction of pure DNA hydrogels for the first time by using branched DNA nanostructures as monomer units together with T4 DNA ligase [6]. Subsequently, several enzyme-based methods for production of DNA hydrogels have been developed, such as rolling circle amplification [7–9]. Enzyme-free formation of DNA hydrogels and DNA-nanomaterial composite hydrogels has also been demonstrated. While DNA hydrogels have been successfully produced using multiple strategies [10], to our knowledge, no DNA-based aerogel has previously been reported. Aerogels are low-density, highly-porous (>90%) materials with potential uses in diverse technologies and are conventionally fabricated via multiple solvent exchange steps followed by complicated solvent removal [11–13]. Here, we report fabrication of DNA aerogels through direct freeze-drying of DNA hydrogels via a facile and environmentally friendly method, without the need for complicated steps or organic solvents. Understanding of the self-assembly of DNA to create aerogels may pave the way to construct novel aerogel-based material platforms from DNA coated or wrapped functional moieties. We illustrate this direction herein using DNA-wrapped CNT aerogels.

Previously, we constructed pure DNA hydrogels using Y-shaped or X-shaped DNA tiles and dsDNA linkers [14]. In this study, DNA hydrogels are converted to pure DNA aerogels via a freeze-drying process as displayed in the schematic in Fig. 1a. We adopted sequences of strands used previously to construct Y-shaped DNA tiles and hydrogels [15]. Complementary strands dissolved in buffer were annealed using a heating and cooling process. Thus single-strand DNA sticky-ends containing address codes oriented and attached to neighboring substructures in three-dimensions (3D) and formed a hydrogel. The DNA hydrogel was

* Corresponding author.
** Corresponding author.
E-mail addresses: khan@eos.ncsu.edu (S.A. Khan), thlabean@ncsu.edu (T.H. LaBean).

https://doi.org/10.1016/j.mtbio.2022.100440
Received 24 July 2022; Received in revised form 22 September 2022; Accepted 24 September 2022
Available online 26 September 2022

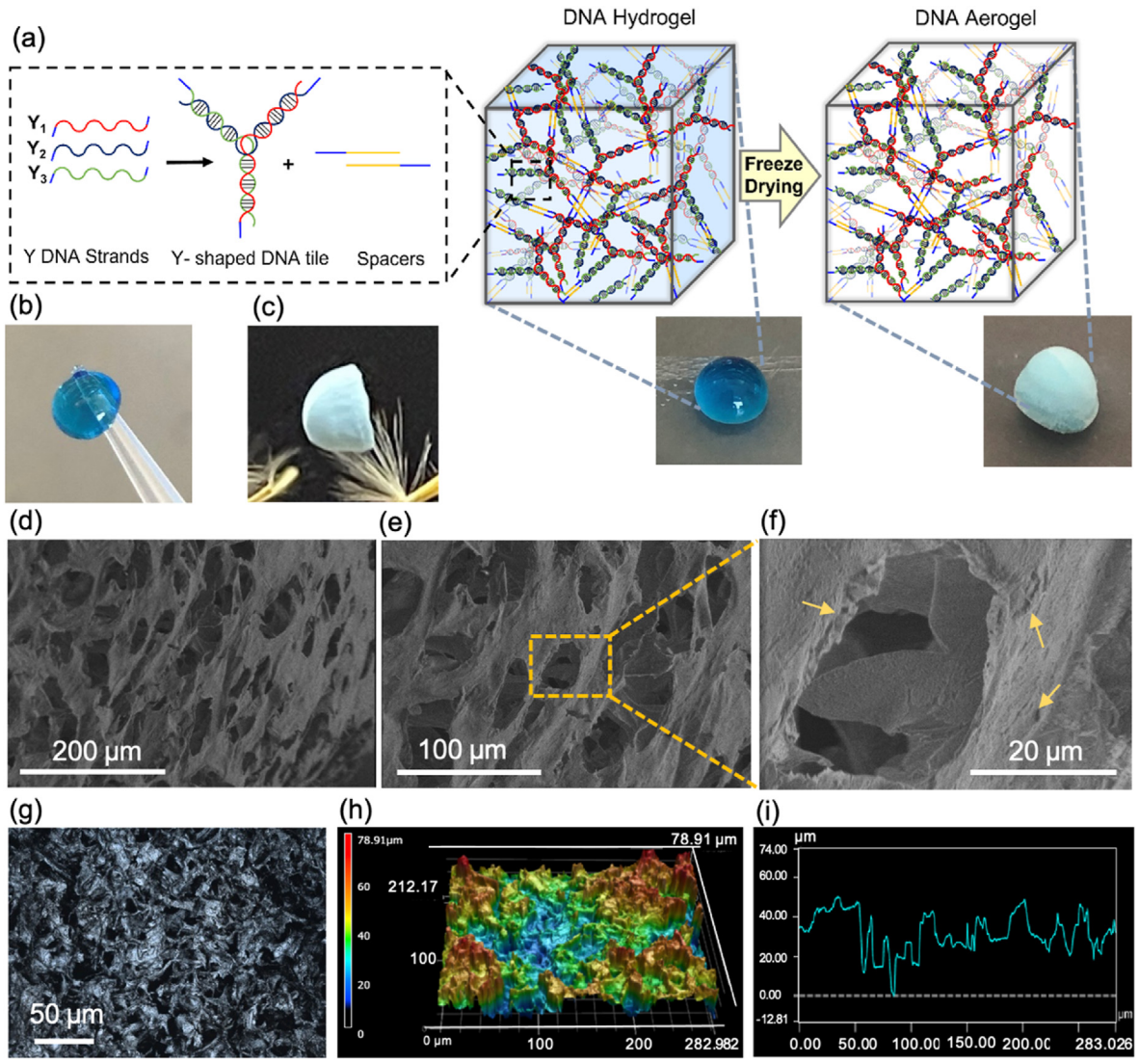

Fig. 1. Fabrication and morphology of pure DNA aerogel. (a) Schematic illustration of the Y-DNA aerogel formation. Three single-stranded DNA strands are mixed to form Y-shape DNA tiles, followed by combination with DNA spacer to form 3D random DNA hydrogel. The spacers are also in a helical structure, but to be distinguishable in the illustration, are depicted as straight lines, with the small blue segments representing the sticky-ends. Finally, the hydrogel is frozen and freeze-dried to generate DNA aerogel. The photographic images on the bottom of schematic show DNA hydrogel and aerogel associated with the respective schematic. Photographs of (b) DNA gel droplet on a pipette tip. (c) DNA aerogel supported on light pampas grass plume. SEM images of DNA aerogel (d) surface structure with hierarchical porous architectures, (e) zoomed-in image of the surface. (f) High magnification image of the DNA aerogel showing a pore and uneven surface of the wall (yellow arrows). (g) Confocal laser scanning micrograph of the cross-section of DNA aerogel. (h) Depth profile image and, (i) graph of a cross-section of pure DNA aerogel showing uneven surface and inhomogeneous size and depths of the pores in the aerogel.

subsequently freeze-dried over 48 h to remove water and produce ultralight and highly porous DNA aerogel. The unique feature of our aerogel fabrication approach is the direct transformation of the DNA hydrogel to aerogel by sublimation of ice crystals without requiring solvent exchange, resulting in a more straightforward, cost-effective, and sustainable process. This contrasts with the complicated conventional aerogel fabrication, which relies on organic solvents which are used in multiple solvent exchanges to preserve the integrity of the gel network structure during solvent removal by critical point drying.

The gel state of a DNA hydrogel is demonstrated on the pipette tip in the image shown in Fig. 1b. For better visualization and insight into the structure of our aerogel, a blue dye (xylene cyanol FF) was added to the DNA hydrogel. Freeze-drying the hydrogel to replace the solvent with air results in a low-density aerogel visually verified by it being supported on a fragile object (such as pampas grass plume) without affecting its shape as shown in Fig. 1c. During freezing of the hydrogel, the growing ice crystals may orient the polymeric strands between the crystals, thus resulting in a porous, cellular structure. Since the space between the interconnected DNA chains is occupied by air, the resultant aerogel has low density; in this case, approximately 0.125 ± 0.002 g cm^{-3}. The porous structure of the aerogel can be easily seen by scanning electron microscopy (SEM) as shown in Fig. 1d–f. SEM images of DNA aerogel at different magnifications display an architecture with high porosity and random pores with average diameter as large as 20–30 µm. These large pores surrounded by a wall constituted by a continuous network of DNA (on this length-scale) are produced as a result of sublimation of solvent water during the freeze-drying process. Additionally, high-resolution SEM image shown in Fig. 1f indicates a highly porous aerogel wall consisting of tiny nanoscale pores (indicated by arrows in Fig. 1f). Hierarchical porosity, as previously described in other aerogels [16], of our DNA aerogel was further verified via confocal laser scanning microscopy, as shown by the micrograph of a DNA aerogel cross-section in Fig. 1g. In addition, the depth profiling of the cross-section of DNA aerogel (shown as an image and corresponding graph in Fig. 1h and i) illustrate the

porous nature of the aerogel. While the depth of the aerogel in the depth profile plot is arbitrarily fixed at zero (dotted line in Fig. 1i), it indicates an inhomogeneous surface consisting of multiple tiny pores with a variety of sizes (depths) contributing to the roughness of the aerogel cell wall.

The pure DNA aerogel demonstrates a random, porous 3D structure; however, we can exploit DNA's biomolecular assisted self-assembly to control hierarchical architectures and change topology or average connectivity at different structural levels. Porous DNA aerogel structure with high surface area provides enough space and adhesion for nanomaterials to interact and assemble DNA conjugate building blocks to design mechanically and electrically adaptable nanocomposites. Hence, we investigated the ability of DNA appendant to nanoscale materials to act as "smart glue" for construction of functional aerogels. These novel aerogels can serve as a platform for developing complex 3D nano-electronic materials, devices, or networks for future neuromorphic applications [17]. Neuromorphic systems have attracted a lot of interest in recent years as a means to overcome some limitations of current semiconductor lithographic fabrication technology, such as physical scaling limits in two-dimensional (2D), a lack of 3D integration, and low energy efficiency of devices, by mimicking some aspects of biological neural network systems [18–20].

Among nanoscale materials, CNTs are a popular conducting/semiconducting nanomaterial for use in self-assembled devices and circuits. CNT has shown great potential in electronics, optics, mechanics, thermal transportation, and biosensing [21,22]. CNTs have been used to form electrically conductive and highly interconnected percolating networks as structural nanocomposites for nanoelectronics applications [23]. In addition, the role of CNTs in molecular electronics as non-volatile random-access memory has also been reported [24,25]. When CNT films have been placed between two electrodes, they have shown resistive switching behavior or memristivity [26] as well as exhibiting strong nonlinear, Schottky characteristics [27]. Moreover, pure CNT aerogels' functionalities and applications have been reported previously, along with testing aerogels' mechanical and electrical properties [28–31]. Highly fluorescent solution-free single-walled carbon nanotubes (SWCNTs)-silica aerogels and their photophysical properties has also been studied by Duque et al. [32]. On the other hand, without functionalization or added surfactant, CNT has low dispersibility in aqueous solutions [33], as is seen in Fig. S1. However, SWCNTs can be easily dissolved in an aqueous solution when coated with DNA [34]. DNA-wrapped CNTs are created by non-covalent π-π stacking interactions between DNA nucleobases and CNT walls, resulting in helical wrapping around the surface resulting in the formation of a water-soluble molecular complex [35,36]. It is worth mentioning here that in previous studies, adjusting the electrical properties of hybrid DNA hydrogels embedded with conductive or semiconductive nanomaterials [37] have not been attractive due to undesired ionic conduction within the aqueous phase of the hydrogels [14]. However, to the best of our knowledge, no previous study has reported the fabrication of functional DNA-CNT composite aerogels, in which ionic conduction will be inhibited.

Herein, by applying techniques such as self-assembly and freeze-drying, the unique DNA-CNT aerogels containing random networks of artificial, neuromimetic materials with macro-scale dimensions and nano-scale features were formed and their non-linear electrical behaviors were explored. Fig. 2a shows the steps necessary to fabricate DNA-wrapped SWCNT hydrogel and aerogel. The ability for DNA to wrap CNT has been established in our prior work [14]. A complementary approach in this regard would be to use Raman and photoluminescence to evaluate the micro-environment around CNT [38]; however, such a study falls outside the scope of our current work. We applied semiconductor, single-walled (6,5) chirality CNTs (SWCNT) to wrap DNA strands around by using DNA sequence in Table S1. After annealing and cooling, DNA-CNT hydrogel formed, as illustrated in schematic and digital images in Fig. 2a. As negative control, CNT dispersions in water do not produce aerogels on freeze-drying as shown in Fig. S1. DNA-CNT hydrogel was converted to an aerogel via freeze-drying as shown in the right inset of Fig. 2a.

SEM images of as-prepared hybrid DNA-wrapped SWCNT aerogel at different magnifications in Fig. 2b–f presents a hierarchical morphology containing interconnected DNA-CNT porous structure. Fig. 2b depicts high-resolution interconnected networks of tiny ropes containing CNT and DNA strands. The cellular nature of the aerogel is illustrated in Fig. 2c, which also exhibits very thin random strands indicated by arrowheads on the surface of the wall. A noticeable difference between the morphology of the pure DNA aerogel in Fig. 1d–f and DNA-CNT aerogel in Fig. 2d–f is that the pure DNA aerogel exhibits more distinct pores with a higher pore density. In addition, compared to the comparatively uneven walls of the DNA aerogels, DNA-CNT aerogels exhibit smoother walls with larger pores and sharp edges, yielding a truly interconnected, open porous network that may have the capacity to enhance the system's functionality. The depth profile of the DNA-CNT hybrid aerogel (Fig. 2i) also shows a rougher structure with deeper pores (~138 μm to the baseline) as compared to those of DNA-only aerogel (~79 μm as shown in Fig. 1i). A comparison between the roughness (brought out by the surface pores) of the cross-sections of the pure DNA aerogel and DNA-wrapped CNT aerogel further strengthens our argument since the values of mean height, maximum height, mean peak curvature, and developed interfacial area ratio, listed in Table 1, are higher for DNA-CNT hybrid aerogels than the DNA-only aerogels, indicating a rough structure with deeper pores. The differences in the structure of the two systems stems from the inherent difference in the length scales of DNA and CNT. The length of the DNA is in the nanoscale whereas that of CNT is in the micron range. DNA aerogel thus provides a densely packed structure with smaller pores in comparison to CNT-DNA hybrid aerogel comprised of larger pores.

It has been reported that memristors (2-terminal memory devices functioning based on resistive switching phenomena) are promising candidates for neuromorphic computing [39]. These DNA-CNT hybrid aerogels may be useful as self-assembled memristive materials due to their resistive switching behavior, and they may serve a neuromorphic hardware role in nanoelectronics circuits. To investigate the electrical characteristics of DNA-CNT aerogel, the current-voltage (IV) measurements were performed after required preparation steps as explained in detail in the supplementary information (Figs. S2–S4). Specifically, a 3 × 3 microelectrode array was inserted into the hydrogel in a vial prior to placing it in the freeze-dryer to form the aerogel in the shape of the vial's bottom. Thereby, the electrode arrays were fixed at stable, although random locations within the stochastic DNA-CNT network of the aerogel (Fig. S4). The distal ends of the electrodes were inserted in a zero-insertion force (ZIF) socket that was connected to the electronic circuit where current-voltage (IV) curve measurements were recorded. Fig. 3 shows electrical characteristics of DNA-CNT aerogel and its comparison with the behavior of 2D DNA-CNT conjugate and the pure DNA aerogel. The typical IV curve of memristors is a hysteresis pinch reflective of the resistive switching behavior [40]. Here, integral memristance is observed because low-resistive state (LRS) and high-resistive state (HRS) are calculated relative to the particular train of pulses in one polarity and the aerogel plays the role of resistance-change memory devices [41]. The first pinch (red) in rainbow plots of Fig. 3a in which the device is initially in the HRS, indicated as point 1 during the application of positive sweep from 0 to 20 V. The positive current increases gradually then the device switches to LRS, indicated as point 2. After reversing the polarity, the device remembers its steady-state and switches from LRS to HRS (point 3 to 4) in the negative sweep. This pattern is repeated for 100 hysteresis pinches shown in the order of rainbow colors (i.e., ROYGBIV). Resistance variation over 50 cycles is shown in Fig. 3b. During the first few cycles, both HRS and LRS show higher resistance that starts to decrease, while after around the 30th cycle, both states reach a plateau indicating the endurance performance of the device.

As illustrated in Fig. 3c the IV plot characterization shows nonlinear

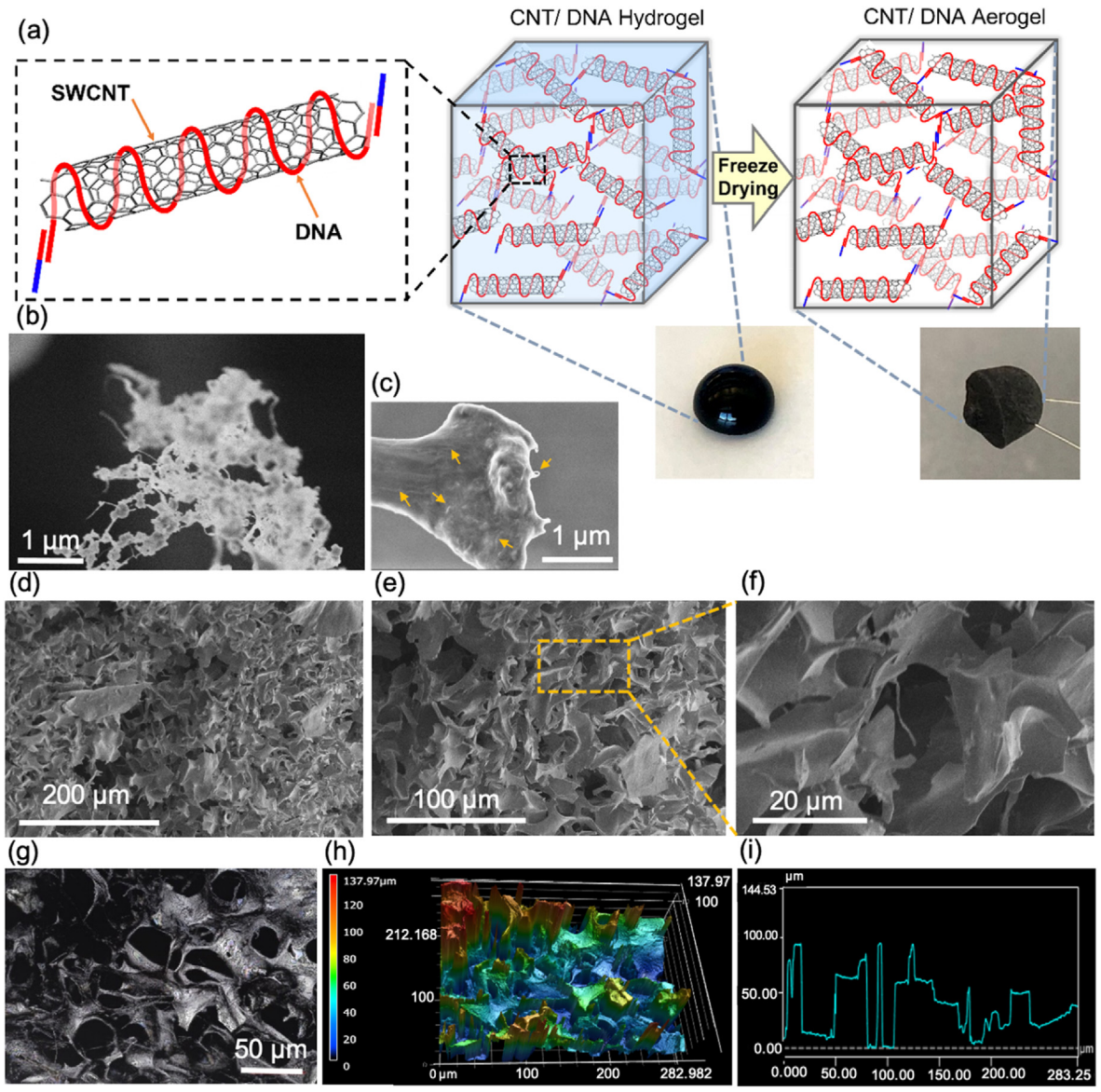

Fig. 2. Fabrication and morphology of DNA-wrapped CNT aerogel. (a) Schematic illustration of the formation process for DNA-wrapped CNT aerogel. SWCNT are sonicated with DNA strands to form the DNA-CNT conjugate, then combined with two different spacer DNAs to form the random DNA-CNT hydrogel. The spacers are also in a helical structure, but to be distinguishable, are depicted in straight lines here. The small blue lines represent the sticky ends. Finally, the frozen hydrogel is freeze-dried to generate DNA-CNT aerogel. The digital images connected to the schematic show respective DNA hydrogel and aerogel. (b) SEM image of tiny ropes containing multiple DNA strands and carbon nanotube. (c) SEM image of a part of the DNA-CNT aerogels wall showing thin ropes on the surface (indicated by arrowheads). (d) The surface structure with porous hierarchical architectures, (e) zoomed-in image with 100 μm scale bar. (f) A high magnification SEM image showing a large pore of DNA-CNT aerogel. (g) Confocal microscopy image of the cross-section area of DNA-CNT aerogel with 50 μm scale bar. h, Depth profile image and, (i) graph showing comparatively more homogeneous surface and deeper pores in the cross-section of DNA-CNT aerogel.

Table 1
Pore characteristics of the pure DNA and DNA-CNT aerogel determined through laser confocal profiling (Figs. 1g and 2g).

	Mean height (μm)	Maximum height (μm)	Mean peak curvature (1/mm)	Developed interfacial area ratio
Pure DNA aerogel	10.55 ± 0.39	78.91 ± 4.81	19219.61 ± 4861	11.11 ± 3.73
DNA-wrapped CNT aerogel	21.95 ± 3.23	137.97 ± 9.86	52813.39 ± 3199	97.84 ± 21.4

behavior with 40 consecutives positive (0–20 V) voltage sweeps. The current continuously increases as the black arrow's direction shows in Fig. 3c. The inset plot shows 40 consecutive negative (0 to −20 V) voltage sweeps which also have incremented in the order of the loops. This behavior can also be observed by plotting current/voltage versus time, as shown in Fig. 3d for six periods of 20 consecutive positive and negative triangle pulse voltage sweeps. These observed nonlinear phenomena can be interpreted as differential, volatile memristivity caused by resistance evolution between the random networks of CNTs and DNA. This resistive switching behavior may also be due to the movement of the CNTs under the influence of electric field and tube charging which can vary the distance within tube-tube junctions leading to changes in current [42]. Further experiments such as the power spectrum profiles of aerogels with CNT networks of similar volumetric concentrations, but different

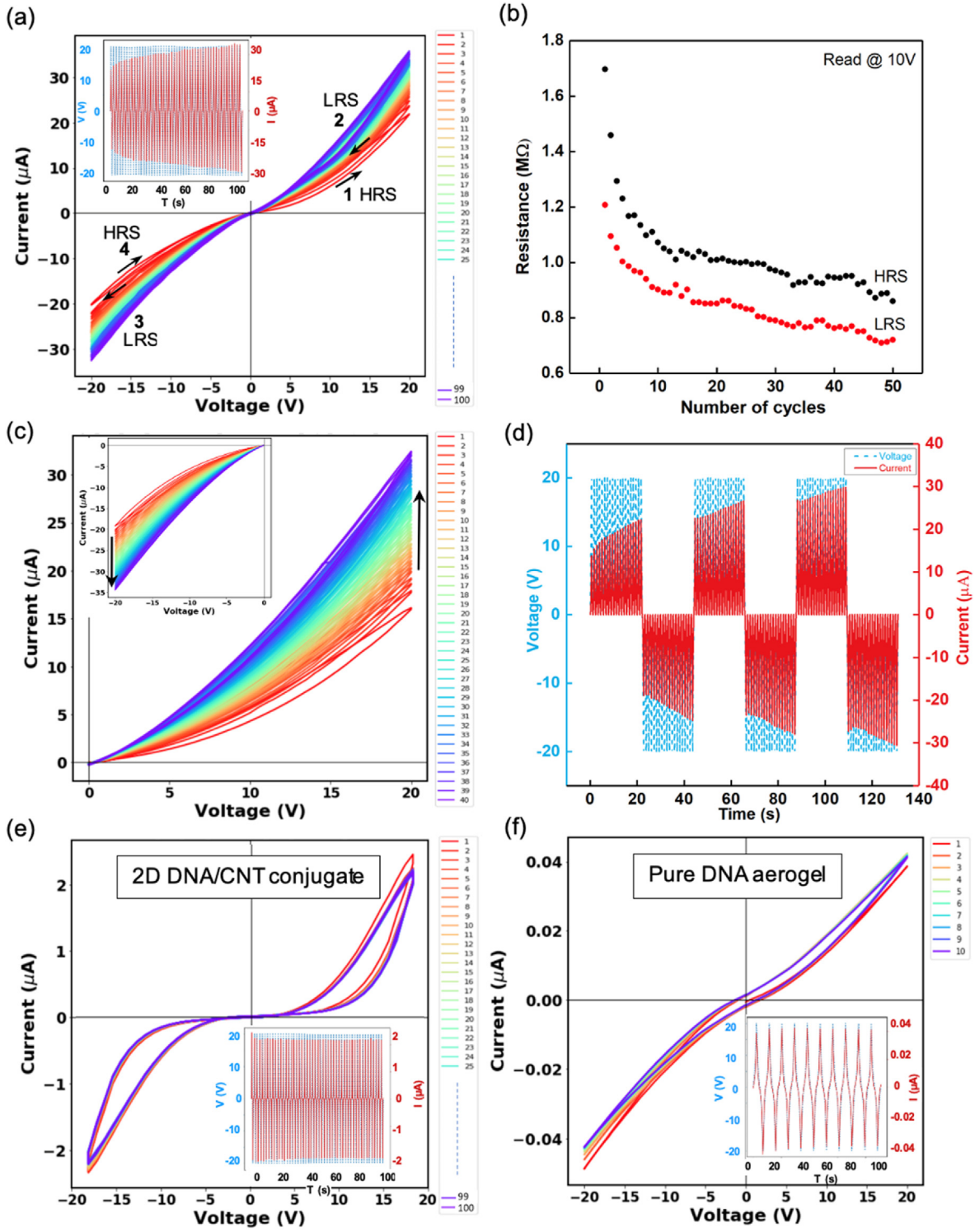

Fig. 3. Nonlinear electrical transmission characteristics of DNA and DNA-CNT aerogels. (a) Typical IV behavior of DNA-CNT aerogel, showing the hysteresis pinch as a fingerprint of memristors. The inset exhibits the input voltage triangle pulses (in dotted blue lines) and outputs current responses (in solid red lines) versus time. (b) DNA-CNT aerogel 's resistance variation versus the number of cycles to show the endurance performance of HRS and LRS over 50 cycles, read at 10 V. (c) IV characteristics of the memristor at positive bias voltage, the voltage sweep range is 0–20 V. The inset shows the negative bias voltage, with voltage sweep range from 0 to −20 V. (d) Six periods of 20 consecutive positive and negative triangle pulse voltage sweeps. The dotted blue lines are input voltage triangle pulses, and the solid red lines are the output current. These observed nonlinear phenomena are somewhat similar to neuronal synapse characteristics that are excited by positive or negative stimulation. (e) Nonlinear IV characteristic of 2D thin film of DNA-CNT conjugates between gold electrodes, which has a small current and no increment during subsequent loops. (f) Nonlinear IV characteristics of pure DNA aerogel does not show a hysteresis pinch and is similar to the capacitor characteristic due to the existence of insulator DNA matrix between the electrodes.

densities of the gels can be derived and compared. The difference in the scaling will provide promising clues in describing the switching behavior.

To confirm the differential memristive behavior of DNA-CNT aerogel, its typical hysteresis IV curve in Fig. 3a was compared to those from two different structures. First, 2D DNA conjugated CNT between gold electrodes was measured after solvent evaporation, in the setup illustrated in Fig. S5. Its result shown in Fig. 3e implies that the 2D thin film of DNA conjugated CNT displays memristive behavior at low current. In addition, there is no increment in the order of the loops with all the hysteresis pinches overlapping. As is illustrated in the voltage/current versus time plot in the inset of Fig. 3e, the overall current does not increase, but rather decreases after around 100 s. Additionally, the pure DNA aerogel (Fig. 3f) does not show memristive behavior since the IV plot is not a complete pinch. It resembles simple capacitive IV characteristics with a small current. The inset plot in Fig. 3f does not show any set process over time, since there is no increase in the overall output current of the device (solid red signals). This signifies that the presence of insulator DNA aerogel between the electrode legs does not have any effect on electrical measurements and yields this capacitor-like behavior. Comparing IV characteristics of pure DNA aerogel and DNA-CNT aerogel confirms the existence of random networks of DNA strands wrapped around the semiconductor CNTs in DNA-CNT aerogel to show the volatile memory feature. When stability of DNA-CNT aerogel's structure and properties over time are examined (Fig. S6), it shows that DNA-CNT aerogel preserved in a dry state maintained its memristive behavior over months, while the unpreserved sample illustrates linear ohmic IV characteristics due to the shrinkage and collapse of CNT nanostructures.

While these results are exciting as proof of concept, several issues need to be addressed to make this a viable option. For instance, a quantification of the DNA wrapping on CNT and how it reflects on properties would be beneficial in limiting DNA use and understanding the process. Such measurements can be obtained using fluorescence-modified DNA [43] and form part of ongoing efforts in our laboratory. And while the current scope of these aerogels does not require enhanced mechanical performance, we intend to investigate the mechanical strength of these aerogels using dynamic mechanical analysis as described by various research groups including ours [44,45] as part of the future. Finally, while our laboratory facility can produce large aerogels, the high price of DNA needs to be taken into consideration when considering scalability. The price of DNA however seems to be on a downward trajectory in the past decade, and the myriad of application possibilities may outweigh such cost issues.

In summary, we present here solvent-free and time-expeditious fabrication of novel DNA aerogels, followed by exploitation of the self-assembly of DNA in coating and wrapping of nanomaterials to construct functional DNA-CNT aerogels. Such systems with porous morphologies and randomly self-assembled networks have potential for use in various applications including biochemical sensing, biodegradable functional implants and nanocircuits for memristors. This approach provides flexibility to tailor morphologies by varying composition and processing parameters such as the nature and content of DNA strands and the nanoparticles in the hydrogel, as well as the rate and direction of freezing. We harnessed the solubility and adaptability of DNA conjugated CNT, the molecular recognition and tunable properties of DNA strands, and the mechanical and electrical properties of CNT and CNT aerogels to construct functional hybrid DNA-CNT aerogels. By removing the water via freeze-drying, self-assembled, 3D constructed, and highly porous DNA-CNT aerogels exhibited impressive electrical behavior that opens new possibilities in nanoelectronics and neuromorphic applications. In particular, DNA aerogels with stochastic superstructures can be combined with specific nanostructures such as DNA origami [46] and other DNA-functionalized nanomaterials to create materials engineered on multiple length-scales. These novel materials have potential for use in 3D integrated circuits with extremely high connectivity that will be developed for real-time computation, communications, analog/mixed-signal processing, and machine learning applications.

1. Methods

1.1. Materials

DNA hydrogel is composed of oligonucleotides that were purchased from Integrated DNA Technologies (IDT, Coralville, IA, USA) with standard desalting and no further purification was required prior to use. Table S1 lists the nucleotide sequences. Tris base (tris(hydroxymethyl) aminomethane, Fisher Scientific), sodium chloride (NaCl, >99.5%, Sigma-Aldrich, St. Louis, MO, USA), HEPES (4-(2-hydroxyethyl)-1-piperazineethanesulfonic acid) (>99.5%, Sigma-Aldrich, St. Louis, MO, USA), and sodium hydroxide (NaOH, >98%, Sigma-Aldrich) were used to make buffer solutions. Single-walled carbon nanotubes (6,5) chirality, (SWNTs; 0.78 nm average diameter; 1 μm median length) were purchased from Sigma-Aldrich (773,735, St. Louis, MO, USA), Nitric acid (ACS reagent, Sigma-Aldrich) and hydrochloric acid (ACS reagent, Sigma-Aldrich) were used to make aqua regia. Xylene Cyanol FF (Sigma-Aldrich- X4126- 10G). Milli-Q deionized (DI) water (>18 MΩ cm resistivity) was used for all experiments.

1.2. Fabrication of Y-shaped DNA tiles and spacers

To specify the molecular assembly instructions for both types of the aerogels, specific DNA sequence recognition is used within the internal structure of the DNA networks, as it is seen in the architectural schematics in Figs. 1a and 2a and listed in Table S1. The sequence of strands to construct Y-shaped DNA tiles and spacers were adopted from previous studies [14,15]. For both fabrications, we used a folding buffer solution (20 mM Tris-HCl (pH 7.5) and 100 mM NaCl) to control the pH, while pH values of the buffers were measured with a standard pH meter (Mettler Toledo SevenEasyTM, Columbus, USA). To construct Y-shaped DNA tiles, 10 μL of 10 mM Y1, Y2, and Y3 precursor strands was added to buffer to obtain a final concentration of 1 mM for each strand. Then, the mixture went through a heat-annealing process (Techne TC-3000 PCR Thermal Cycler) where it was heated to 95 °C for 5 min and then cooled down to room temperature over 30 min. To construct spacers, 15 μL of 10 mM L1, and L2 precursor strands was mixed in the folding buffer (to obtain a final concentration of 1.5 mM for each strand). The mixture then went through the same heat-annealing process described above for DNA tiles.

1.3. Fabrication of pure DNA hydrogel

To fabricate pure DNA hydrogel, the self-assembled Y-DNA tiles and spacers with desired volumes, based on concentrations and ratios, were mixed on the piece of parafilm immediately, and the hydrogel was formed in a minute, then it was transferred to polypropylene tubes and immediately preformed electrical measurements or freeze-drying. Based on the above concentrations for Y-DNA tiles and spacers, a 1:1 ratio of volume is required to form the gel, for example, 10 μL of Y-DNA tiles and 10 μL spacers. For a better insight into the structure, 1 μL suspension of Xylene Cyanol FF with 1.5 mg/ml concentration was added to the DNA hydrogel.

1.4. Formation of DNA–CNT conjugate and hydrogel

Two DNA strands, C1 and C2, were required to construct the DNA-wrapped CNT conjugate. C1 was adopted from a previous study to wrap the SWCNTs with DNA based on the multiple repeated $(GT)_{20}$ units [42]. We modified C2 sequence with our sticky end to make it compatible with spacers [14]. The method was mixing 120 μL HEPES buffer (final concentration 50 mM, pH 7.6) and 1.2 mg CNTs together. Then, 15 μL of 10 mM DNA strand C1 was added. The mixture was sonicated in an

ice-water bath for 30 min using a 100 W bath sonicator. In the end, 15 μL of 10 mM DNA strand C2 was added, and the final solution was incubated at room temperature overnight and then stored in the fridge at 4 °C as the stock.

To fabricate DNA-CNT hydrogel, the DNA-CNT conjugate stock and spacers stock were mixed on the piece of parafilm based on the desired concentration and ratio to form the DNA-CNT hydrogel.

1.5. Fabrication of DNA and DNA-wrapped CNT aerogels

After we prepared the DNA and DNA-CNT hydrogel to fabricate the aerogel, we transferred the gels to polypropylene Eppendorf tubes and placed the microelectrode arrays in the sample to have fixed measurement's points, then cover the cap with a small piece of tissue wiper and transferred the vial into the stoppering tray of freeze-dryer (Labconco FreeZone 6 L system) at ~ 0.003 mbar and −85 °C for 48 h. Finally, to preserve the sample from shrinkage due to air exposure as explained in detail in Figs. S2 and S3, we immediately seal the cap of the vial with epoxy to protect the sample's structure and properties as displays in Fig. S4.

1.6. Characterization of the aerogel morphology

The morphologies of the aerogels were visualized through a field-emission scanning electron microscope (FESEM) (Verios 460 L scanning electron microscope), which is an ultra-high-resolution Schottky emitter SEM. SEM samples were imaged without sputter coating to avoid potential metal coating artifacts. Immediately after removing the sealed cover of the vial, the aerogel was placed into the SEM chamber. Fig. 1d, e, and 2b-e were taken by this method. Moreover, we used a Confocal Laser Scanning Microscope (CLSM) (Keyence VKx1100) to combine optical microscopy with laser profilometry to obtain high-resolution optical images and subsequently measure depth profile and surface roughness. Fig. 1f–i and 2f-i and the information in Tale 1 were taken by CLMS. Pore characteristics were determined with the help of MultiFileAalayzer software by Keyence. Each measurement is an average of ten replicate samples consisting of multiple pores scanned under similar magnification.

1.7. Microelectrode arrays and electrical measurements

We fabricated inexpensive micro-electrode arrays in the lab. The microelectrode arrays are manufactured with Millennia surgical steel acupuncture needles that are 120 μm in diameter and 25 mm in length. The manufacturing setup is straightforward based on the needle alignment with a custom-made laser-drilled steel plate grid containing 6 × 6, 140 μm diameter holes with 100 μm center-to-center spacing. After inserting the needles in holes and aligning, the middle part of aligned needles is covered by insulating two-component epoxy (J-B Weld), and after solidification, ends of arrays are inserted in the custom-made adaptor board with ZIF socket to connect to the electrical circuit. To perform IV curve measurement, the sample was connected to a socket board in a Hewlett Packard Test Fixture Analyzer (16058A, Palo Alto, CA, USA) connected to a 2-channel (medium-power) source/monitor unit module (Agilent Technologies E5272A, Santa Clara, CA, USA).

Credit author statement

Mahshid Hosseini: Conceptualization, Methodology, Investigation, Formal Analysis, Validation, Writing-Original Draft. **Vahid Rahmanian**: Conceptualization, Methodology, Investigation, Formal Analysis, Validation, Writing- Reviewing and Editing. **Tahira Pirzada**: Conceptualization, Methodology, Investigation, Formal Analysis, Validation, Writing- Reviewing and Editing. **Nikolay Frick**: Methodology, Validation, Writing- Reviewing and Editing. **Abhichart Krissanaprasit**: Conceptualization, Validation, Writing- Reviewing and Editing. **Thomas H. LaBean:** Conceptualization, Writing- Reviewing and Editing, Supervision, Project Administration. **Saad A. Khan**: Conceptualization, Writing- Reviewing and Editing, Supervision, Project Administration.

Declaration of competing interest

The authors declare that they have no known competing financial interests or personal relationships that could have appeared to influence the work reported in this paper.

Data availability

Data will be made available on request.

Acknowledgments

The authors acknowledge support for this research from the National Science Foundation through award NSF-CISE-CCF 1748459 to T.H.L. The authors also thank Dr. E. Vetter for fabrication of two-dimensional gold electrodes. This work was performed in part at the Analytical Instrumentation Facility (AIF) at North Carolina State University, which is supported by the State of North Carolina and the National Science Foundation (award number ECCS-2025064). The AIF is a member of the North Carolina Research Triangle Nanotechnology Network (RTNN), a site in the National Nanotechnology Coordinated Infrastructure (NNCI).

Appendix A. Supplementary data

Supplementary data to this article can be found online at https://doi.org/10.1016/j.mtbio.2022.100440.

References

[1] N. Seeman, DNA in a material world, Nature 421 (6921) (2003) 427–431, https://doi.org/10.1038/nature01406.
[2] H. Li, J.D. Carter, T.H. LaBean, Nanofabrication by DNA self-assembly, mater, Today Off. 12 (5) (2009) 24–32, https://doi.org/10.1016/S1369-7021(09)70157-9.
[3] P. Wang, G. Chatterjee, H. Yan, T.H. LaBean, A.J. Turberfield, C.E. Castro, G. Seelig, Y. Ke, Practical aspects of structural and dynamic DNA nanotechnology, MRS Bull. 42 (12) (2017) 889–896, https://doi.org/10.1557/mrs.2017.272.
[4] S. Douglas, H. Dietz, T. Liedl, B. Högberg, F. Graf, W.M. Shih, Self-assembly of DNA into nanoscale three-dimensional shapes, Nature 459 (7245) (2009) 414–418, https://doi.org/10.1038/nature08016.
[5] A.N. Marchi, I. Saaem, B.N. Vogen, S. Brown, T.H. LaBean, Toward larger DNA origami, Nano Lett. 14 (10) (2014) 5740–5747, https://doi.org/10.1021/nl502626s.
[6] S.H. Um, J.B. Lee, N. Park, S.Y. Kwon, C.C. Umbach, D. Luo, Enzyme-catalysed assembly of DNA hydrogel, Nat. Mater. 5 (10) (2006) 797–801, https://doi.org/10.1038/nmat1741.
[7] J.B. Lee, S. Peng, D. Yang, Y.H. Roh, H. Funabashi, N. Park, E.J. Rice, L. Chen, R. Long, M. Wu, D. Luo, A mechanical metamaterial made from a DNA hydrogel, Nat. Nanotechnol. 7 (12) (2012) 816–820, https://doi.org/10.1038/nnano.2012.211.
[8] J. Bush, C.H. Hu, R. Veneziano, Mechanical properties of DNA hydrogels: towards highly programmable biomaterials, Appl. Sci. 11 (4) (2021) 1885, https://doi.org/10.3390/app11041885.
[9] C. Yao, R. Zhang, J. Tang, D. Yang, Rolling circle amplification (RCA)-based DNA hydrogel, Nat. Protoc. 16 (12) (2021) 5460–5483, https://doi.org/10.1038/s41596-021-00621-2.
[10] Y.A. Pardo, K.G. Yancey, D.S. Rosenwasser, D.M. Bassen, J.T. Butcher, J.E. Sabin, M. Ma, S. Hamada, D. Luo, Interfacing DNA hydrogels with ceramics for biofunctional architectural materials, Mater. Today 53 (2022) 98–105, https://doi.org/10.1016/j.mattod.2021.10.029.
[11] S. Zhao, W.J. Malfait, N. Guerrero-Alburquerque, M.M. Koebel, G. Nyström, Biopolymer aerogels and foams: chemistry, properties, and applications, Angew. Chem. Int. Ed. 57 (26) (2018) 7580–7608, https://doi.org/10.1002/anie.201709014.
[12] H.Z. Sai, R. Fu, L. Xing, J.H. Xiang, Z.Y. Li, T. Zhang, F.S. Zhang, Cellulose-silica composite aerogels prepared with sodium silicate by freeze drying method, Key Eng. Mater. 697 (2016) 129–133, https://doi.org/10.4028/www.scientific.net/KEM.697.129.
[13] Z. Mazrouei-Sebdani, H. Begum, S. Schoenwald, K.V. Horoshenkov, W.J. Malfait, A review on silica aerogel-based materials for acoustic applications, J. Non-Cryst. Solids 562 (2021), 120770, https://doi.org/10.1016/j.jnoncrysol.2021.120770.

[14] M. Gao, A. Krissanaprasit, A. Miles, L.C. Hsiao, T.H. LaBean, Mechanical and electrical properties of DNA hydrogel-based composites containing self-assembled three-dimensional nanocircuits, Appl. Sci. 11 (5) (2021) 2245, https://doi.org/10.3390/app11052245.
[15] Y. Xing, E. Cheng, Y. Yang, P. Chen, T. Zhang, Y. Sun, Z. Yang, D. Liu, Self-assembled DNA hydrogels with designable thermal and enzymatic responsiveness, Adv. Mater. 23 (9) (2011) 1117–1121, https://doi.org/10.1002/adma.201003343.
[16] Y. Si, J. Yu, X. Tang, J. Ge, B. Ding, Ultralight nanofibre-assembled cellular aerogels with superelasticity and multifunctionality, Nat. Commun. 5 (1) (2014) 1–8, https://doi.org/10.1038/ncomms6802.
[17] L. Qian, E. Winfree, J. Bruck, Neural network computation with DNA strand displacement cascades, Nature 475 (7356) (2011) 368–372, https://doi.org/10.1038/nature10262.
[18] D. Marković, A. Mizrahi, D. Querlioz, J. Grollier, Physics for neuromorphic computing, Nat. Rev. Phys. 2 (9) (2020) 499–510, https://doi.org/10.1038/s42254-020-0208-2.
[19] V.K. Sangwan, M.C. Hersam, Neuromorphic nanoelectronic materials, Nat. Nanotechnol. 15 (7) (2020) 517–528, https://doi.org/10.1038/s41565-020-0647-z.
[20] A.R. Young, M.E. Dean, J.S. Plank, G.S. Rose, A review of spiking neuromorphic hardware communication systems, IEEE Access 7 (2019) 135606–135620, https://doi.org/10.1109/ACCESS.2019.2941772.
[21] J. Lei, H. Ju, Nanotubes in biosensing, Wiley Interdiscip. Rev. Nanomed. Nanobiotechnol. 2 (5) (2010) 496–509, https://doi.org/10.1002/wnan.94.
[22] K. Chu, D. Kim, Y. Sohn, S. Lee, C. Moon, S. Park, Electrical and thermal properties of carbon-nanotube composite for flexible electric heating-unit applications, IEEE Electron. Device Lett. 34 (5) (2013) 668–670, https://doi.org/10.1109/LED.2013.2249493.
[23] A.V. Kyrylyuk, M.C. Hermant, T. Schilling, B. Klumperman, C.E. Koning, P. Van der Schoot, Controlling electrical percolation in multicomponent carbon nanotube dispersions, Nat. Nanotechnol. 6 (6) (2011) 364–369, https://doi.org/10.1038/nnano.2011.40.
[24] T. Rueckes, K. Kim, E. Joselevich, G.Y. Tseng, C.L. Cheung, C.M. Lieber, Carbon nanotube-based nonvolatile random access memory for molecular computing, Science 289 (5476) (2000) 94–97, https://doi.org/10.1126/science.289.5476.94.
[25] J.W. Kang, J.H. Lee, H.J. Lee, H.J. Hwang, A study on carbon nanotube bridge as a electromechanical memory device, Phys. E: Low-Dimens. Syst. Nanostructures 27 (3) (2005) 332–340, https://doi.org/10.1016/j.physe.2004.12.009.
[26] J. Farmer, W. Whitehead, A. Hall, D. Veksler, G. Bersuker, D. Gao, A.M. El-Sayed, T. Durrant, A. Shluger, T. Rueckes, L. Cleveland, Mitigating switching variability in carbon nanotube memristors, in: IEEE International Reliability Physics Symposium (IRPS), IEEE, 2021, pp. 1–4, https://doi.org/10.1109/IRPS46558.2021.9405123.
[27] H.T. Maune, S.P. Han, R.D. Barish, M. Bockrath, P.W. Rothemund, E. Winfree, Self-assembly of carbon nanotubes into two-dimensional geometries using DNA origami templates, Nat. Nanotechnol. 5 (1) (2009) 61–66, https://doi.org/10.1038/nnano.2009.311.
[28] J. Zou, J. Liu, A.S. Karakoti, A. Kumar, D. Joung, Q. Li, S.I. Khondaker, S. Seal, L. Zhai, Ultralight multiwalled carbon nanotube aerogel, ACS Nano 4 (12) (2010) 7293–7302, https://doi.org/10.1021/nn102246a.
[29] H. Sun, Z. Xu, C. Gao, Multifunctional, ultra-flyweight, synergistically assembled carbon aerogels, Adv. Mater. 25 (18) (2013) 2554–2560, https://doi.org/10.1002/adma.201204576.
[30] M.B. Bryning, D.E. Milkie, M.F. Islam, L.A. Hough, J.M. Kikkawa, A.G. Yodh, Carbon nanotube aerogels, Adv. Mater. 19 (5) (2007) 661–664, https://doi.org/10.1002/adma.200601748.
[31] S. Araby, A. Qiu, R. Wang, Z. Zhao, C.H. Wang, J. Ma, Aerogels based on carbon nanomaterials, J. Mater. Sci. 51 (20) (2016) 9157–9189, https://doi.org/10.1007/s10853-016-0141-z.
[32] J.G. Duque, C.E. Hamilton, G. Gupta, S.A. Crooker, J.J. Crochet, A. Mohite, H. Htoon, K.A. Obrey, A.M. Dattelbaum, S.K. Doorn, Fluorescent single-walled carbon nanotube aerogels in surfactant-free environments, ACS Nano 5 (8) (2011) 6686–6694, https://doi.org/10.1021/nn202225k.
[33] S. Vardharajula, S.Z. Ali, P.M. Tiwari, E. Eroğlu, K. Vig, V.A. Dennis, S.R. Singh, Functionalized carbon nanotubes: biomedical applications, Int. J. Nanomedicine 7 (2012) 5361, https://doi.org/10.2147%2FIJN.S35832.
[34] N. Nakashima, S. Okuzono, H. Murakami, T. Nakai, K. Yoshikawa, DNA dissolves single-walled carbon nanotubes in water, Chem. Lett. 32 (5) (2003) 456, https://doi.org/10.1246/cl.2003.456.
[35] A.N. Enyashin, S. Gemming, G. Seifert, DNA-wrapped carbon nanotubes, Nanotechnology 18 (2007), 245702, https://doi.org/10.1088/0957-4484/18/24/245702.
[36] M. Zheng, A. Jagota, E.D. Semke, B.A. Diner, R.S. McLean, S.R. Lustig, R.E. Richardson, N.G. Tassi, DNA-assisted dispersion and separation of carbon nanotubes, Nat. Mater. 2 (5) (2003) 338–342, https://doi.org/10.1038/nmat877.
[37] G. Ma, K. Zhang, H. Wang, Z. Liang, L. Zhou, B. Yan, Versatile synthesis of a highly porous DNA/CNT hydrogel for the adsorption of the carcinogen PAH, ChemComm 57 (18) (2021) 2289–2292, https://doi.org/10.1039/D0CC07066A.
[38] C.A. Silvera-Batista, R.K. Wang, P. Weinberg, K.J. Ziegler, Solvatochromic shifts of single-walled carbon nanotubes in nonpolar microenvironments, Phys. Chem. Chem. Phys. 12 (26) (2010) 6990–6998, https://doi.org/10.1039/B927053A.
[39] Y. Li, K.W. Ang, Hardware implementation of neuromorphic computing using large-scale memristor crossbar arrays, Adv. Intell. Syst. 3 (1) (2021), 2000137 https://doi.org/10.1002/aisy.202000137.
[40] D.B. Strukov, G.S. Snider, D.R. Stewart, R.S. Williams, The missing memristor found, Nature 453 (7191) (2008) 80–83, https://doi.org/10.1038/nature06932.
[41] D. Veksler, G. Bersuker, A.W. Bushmaker, M. Mason, P.R. Shrestha, K.P. Cheung, J.P. Campbell, T. Rueckes, L. Cleveland, H. Luan, D.C. Gilmer, Memory update characteristics of carbon nanotube memristors (NRAM®) under circuitry-relevant operation conditions, in: IEEE International Reliability Physics Symposium (IRPS), IEEE, 2020, pp. 1–4, https://doi.org/10.1109/IRPS45951.2020.9128335.
[42] E. Cheng, Y. Li, Z. Yang, Z. Deng, D. Liu, DNA-SWNT hybrid hydrogel, Chem. Commun. 47 (19) (2011) 5545–5547, https://doi.org/10.1039/C1CC11028D.
[43] K. Umemura, S. Sato, G. Bustamante, J.Y. Ye, Using a fluorescence quenching method to detect DNA adsorption onto single-walled carbon nanotube surfaces, Colloids Surf. B Biointerfaces 160 (2017) 201–206, https://doi.org/10.1016/j.colsurfb.2017.09.029.
[44] T. Pirzada, Z. Ashrafi, W. Xie, S.A. Khan, Cellulose silica hybrid nanofiber aerogels: from sol–gel electrospun nanofibers to multifunctional aerogels, Adv. Funct. Mater. 30 (5) (2020), 1907359, https://doi.org/10.1002/adfm.201907359.
[45] J. Zhang, Y. Cheng, C. Xu, M. Gao, m. Zhu, L. Jiang, Hierarchical interface engineering for advanced nanocellulosic hybrid aerogels with high compressibility and multifunctionality, Adv. Funct. Mater. 31 (19) (2021) 2009349, https://doi.org/10.1002/adfm.202009349.
[46] P.W. Rothemund, Folding DNA to create nanoscale shapes and patterns, Nature 440 (7082) (2006) 297–302, https://doi.org/10.1038/nature04586.